# Statistical Analysis of Surface Reflectivity with GNSS Reflected Signals from a Mixed Ice and Water Surface

Roohollah Parvizi, Shahrukh Khan, *Illinois Institute of Technology*Alison Banwell, *University of Colorado at Boulder*Seebany Datta-Barua, *Illinois Institute of Technology* 

#### **BIOGRAPHY**

**Roohollah Parvizi** is a post-doctoral scholar at Illinois Institute of Technology (IIT). He is working on GNSS reflectometry and GNSS receiver software. He has a Ph.D. in mechanical and aerospace engineering from IIT, and a master's degree in energy systems, specializing in control and thermodynamic modeling of combined heat and power systems.

**Shahrukh Khan** is a Feature owner engineer at Ford Motor company. He is working on development of Advanced Driver Assistance features. Shahrukh has a Master's degree in mechanical and aerospace engineering from IIT with a thesis on camera/lidar sensor fusion, and a bachelor's degree in mechanical engineering from Air University Islamabad.

**Alison Banwell** is a Research Scientist at the Cooperative Institute for Research in Environmental Sciences at the University of Colorado Boulder. She received a Ph.D. (2013) in glaciology from the University of Cambridge, UK. One of her current research interests focuses on surface melt processes on glaciers, ice sheets and ice shelves.

**Seebany Datta-Barua** is an Associate Professor of Mechanical and Aerospace Engineering at Illinois Institute of Technology. She received a Ph.D. (2008) in aeronautics and astronautics from Stanford University. Dr. Datta-Barua researches the use of GNSS for remote sensing. She is the recipient of the 2018 ION Per Enge Early Achievement Award.

# **ABSTRACT**

This paper analyzes the surface reflectivity (SR) over time of GPS L1 signals scattered off a partially frozen lake surface. The SR for a given GPS satellite is compared with the mean red value (MRV) of pixels inside the Fresnel zone taken by collocated cameras, with the MRV serving as a truth reference for water (low MRV) or ice (high MRV). GPS signals are collected during a data campaign at Lake Michigan in Chicago, at a time when the lake surface consisted of a mixture of ice and water. A portable ground-based sensor suite is set up at the lake front to collect both surface-scattered GPS signals and independent validation data (lidar and camera) from the surface.

The camera pixel locations and the Fresnel zone of the GPS satellites are mapped into an east-north-up (ENU) coordinate system centered at the reflected antenna. The MRV of the Fresnel zone is computed for each satellite. Satellites whose Fresnel zones sweep across both water and ice over the lake surface are selected.

To process the GPS reflected signals of chosen satellites, a software defined receiver is customized. In order to find the SNR, one ms coherent correlation power is summed incoherently for one minute for reflected signals. The distance from the satellites to reflection point (Fresnel zone) and from the reflection point to the reflected antenna are computed in order to estimate the SR. Then the SR is correlated with the mean red value. High correlation is seen between SR and MRV for PRN 26, while for PRN 16 only low-to-moderate correlation is found. The low correlation is attributed to a lack of overlap between the Fresnel zone of PRN 16 and the cameras' fields of view.

### I. INTRODUCTION

Although positioning, navigation and timing (PNT) were the initial application of GNSS, its widespread coverage and availability make it a remarkable source for remote sensing purposes, especially of Earth's environment. Generally, GNSS reflected signals are treated as a source of noise, i.e. multipath, in PNT, but they contain information about the surface from which they are reflected [1]. GNSS reflectometry (GNSS-R) has been used to study snow accumulation [2][3], surface moisture [4] [5], wind speed estimation [6], and altimetry from the ground air, and space [6][7] [8].

Sensing surface water phase change between solid and liquid forms for cryospheric science using GNSS reflected signals in particular has been a property of interest. For instant, freshwater lakes can be a major thermal source or sink, influencing

regional weather and the ecosystem. For lakes the cycle of freeze and thaw may vary not only from year to year but also over a matter of days. Another application of interest is in characterizing glacial surface melt. Long-term variation of the cryosphere is related to climate change processes, and short term variations within a season are important as evidence of differential heating of the surface.

Existing earth remote sensing methods such as satellite-based remote sensing methods can provide global coverage but may have limited surface revisit times and coarser resolution than ground-based systems. Depending on the wavelength band they also may be limited to dayside imaging or obscured by cloud cover [9]. For example, the MODerate-resolution Imaging Spectroradiometer (MODIS) instrument on the Terra and Aqua satellites operates in the visible band, has 250 m spatial resolution, and is subject to surface obscuration by clouds [10].

Widespread coverage and availability make GNSS an exceptional source to remotely sense Earth's environment. Leveraging GNSS as a bistatic radar from ground-based or airborne systems has the potential to provide a complementary sensing method of surface water phase. The GNSS signal is unaffected by precipitation and cloud cover and has the potential to have lower cost and higher resolution. GNSS reflectometry (GNSS-R) is the analysis of the scattered signal power and waveform for estimation of the properties of the surface from which they reflect [6] [11].

In the recent past, we developed a ground-based GNSS-R system to study the Earth's environment locally, specifically targeting surface lake water phase changes (between ice and water) [11] [12] [13]. In this work, surface reflectivity (SR) is computed and compared to camera RGB values of the surface to see how the SR varies with reflection surface type. To this end, the mean red value of the pixels inside the Fresnel zone of GPS satellites whose reflection is on the desired surface is computed. The mean red value is used as a "truth" marker of the phase of water, and is correlated with the SR of PRNs that scan across ice and water over time. The objective of this work is to discover whether GNSS-R surface reflectivity may serve as a metric to distinguish ice from water or not. We evaluate two GNSS satellites' signals that scan across the lake surface.

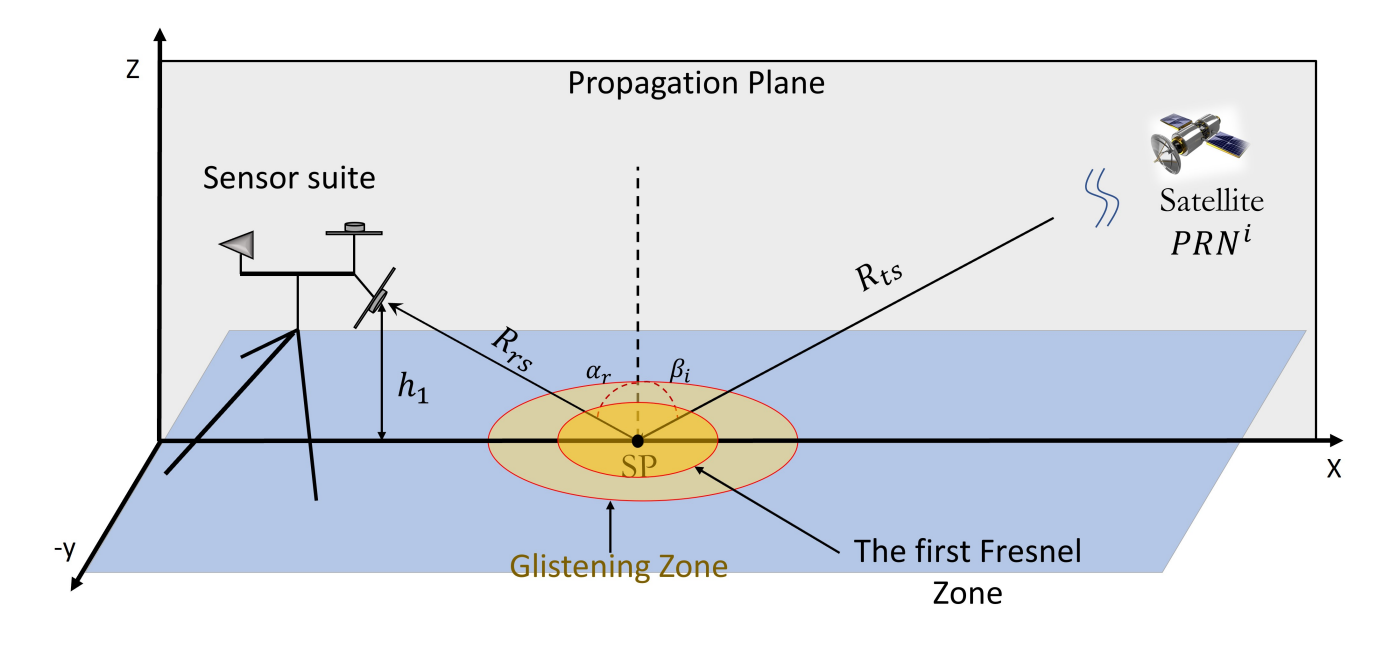


**Figure 1:** Conceptual diagram of GNSS reflectometry.

# II. BACKGROUND

The roughness of a surface relative to the signal wavelength determines whether a signal will be scattered diffusely (in many directions) or specularly (dominantly in one direction). A GNSS signal reflecting from a surface of ice or water is dominated by specular reflection. The specular point (SP) is the point at which the angle of incidence equals the angle of reflection (Figure 1), according to the principle of least time. The glistening zone surrounding the specular point is the area from which both coherent and incoherent components of GNSS reflection scatter, and the size of the glistening zone is a function of the surface roughness. A narrow area around the specular point inside the glistening zone is called the first Fresnel zone, from which the strongest coherent scattering component comes [14] [12]. The phase difference between the GNSS reflection rays arriving at the antenna from the first Fresnel zone is equal to half of the wavelength  $\lambda$  of the signal [15] [14].

Surface reflectivity is the ratio of the incident signal power at a surface to the reflected signal power. The surface reflectivity is related to the received SNR [16] [12] by the radar equation. In decibels, this can be expressed as:

$$SR \propto SNR - 10\log(P_r^t) - 10\log(G^t) - 10\log(G^r) - 20\log(\lambda) + 20\log(R_{ts} + R_{sr}) + 20\log(4\pi)$$
 (1)

where  $G^t$  is the gain of the transmitter,  $G^r$  is the gain of the receiver (reflected antenna gain [12] [11]),  $\lambda$  is the wavelength of the transmitted signal, and  $R_{ts}$ ,  $R_{sr}$  are the distances from the transmitter to scatterer and from the scatterer to the receiver, respectively. The transmitter power  $P_r^t$  and gain  $G^t$  and carrier wavelength  $\lambda$  are known [17], and the receiver gain  $G^r$  can be estimated using the antenna gain pattern (see [12] [11]).

For a given GNSS satellite, the SNR can be computed according to:

$$SNR = \frac{P_{max} - P_{noise}}{P_{noise}} \tag{2}$$

where  $P_{max}$  is the correlation peak value and  $P_{noise}$  is the mean value of the correlation curve excluding the points within one-half chip of the peak ([18]).

The distances  $R_{ts}$ ,  $R_{sr}$  can be estimated given the position of the satellite and the reflected antenna, respectively, relative to the specular point. The position of the specular point on the surface is indicated with  $x_0$  in the propagation plane and the first Fresnel zone area A are computed as follows [15] [14]:

$$d = \frac{\lambda}{2}$$

$$b = \left(\frac{2dh_1}{\sin(e)} + \left(\frac{d}{\sin(e)}\right)^2\right)$$

$$a = \frac{b}{\sin(e)}$$

$$x_0 = \frac{h_1}{\tan(e)} + \frac{\frac{d}{\sin(e)}}{\tan(e)}$$

$$A = \pi ab$$
(3)

In this equation, d is one-half wavelengths and defines the first Fresnel zone. The semi-major and semi-minor axes of the Fresnel zone in the propagation plane (Figure 1) are a and b, respectively. Also, e is the satellite elevation angle and  $h_1$  is the height of reflected antenna relative to the specular point. These equations assume a flat Earth, which is valid for a ground-based antenna system.

# III. METHOD

In this study, we examine whether surface reflectivity of GNSS reflected signals can be used to discriminate ice from water. To this end, we have developed a sensor suite system for monitoring lake surface water phase changes [11] [19] using GNSS signals. During the last 4 years, the sensor system has been used for data campaigns at Lake Michigan [20], most occurring in the winter season [12] to ensure some surface ice. Fieldwork was conducted at Lake Michigan in Chicago, Illinois, in previous winters during periods of completely frozen surface ice or fully ice-free conditions. The most recent data campaign (which we will refer to as "LM Test 11"), was one in which the lake surface had a heterogeneous ice and water surface. In the following subsections, we describe the hardware system and configuration with which data were collected in data campaign LM Test 11. We then describe the processing by which the SR is computed for the signal, then we describe the mapping of the first Fresnel zone onto the camera pixels in east-north-up (ENU) coordinates. The mean red value of the camera pixels inside the Fresnel zone of a given satellite is computed and compared with the satellite-based SR.

# 1. Sensor system

Figure 2 illustrates the sensors used in this portable system. Our sensor suite includes two GNSS antennas, a lidar, three cameras, and a weather station. A single laptop is utilized to command all sensors. Sensor power and communication connections are shown in this Figure. A lidar and three cameras (each spanning different fields of view) sense and image the surface from which the GNSS signal is reflected.

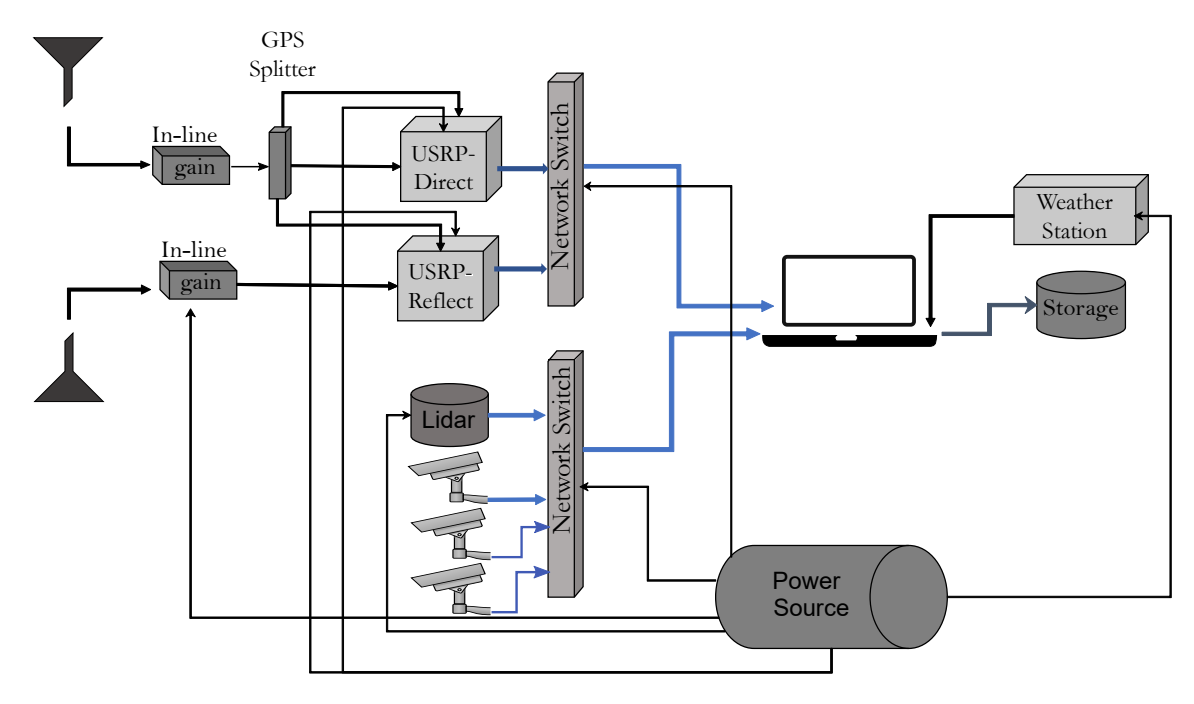


Figure 2: Schematic of the sensor suite.

The lidar and camera data are used to visually determine the surface type in post-processing in the lab. The lidar (a Velodyne "puck") produces a point cloud, estimating sites at which the transmitted laser light is back scattered. The lidar wavelength used reflects off ice but does not reflect from water. The cameras are IP security cameras that produce color images of their field-of-view, which are stored to visually estimate the surface condition at a given point in post-processing. These sensors establish the truth reference of surface ice and water conditions.

Collocated with these sensors are two GNSS antennas. A right-hand circular polarization (RHCP) antenna is used to obtain the direct signal, for basic positioning. A left-hand circularly polarized (LHCP) antenna oriented downwards obtains the reflected GNSS signals from the surface. Two universal software radio peripherals (USRPs, Ettus N210) act as front ends, each of which uses a GPS-disciplined oscillator (GPSDO) connected to the RHCP antenna as a timing reference. One USRP receives the direct GNSS signals from the RHCP antenna for sensor system positioning. The other USRP collects front-end samples from the LHCP reflection antenna. The SNR and SR will be computed from the reflection antenna signal.

A photo of the sensors on the tripod is shown in Figure 3 right. GNSS antennas are mounted on a boom with a direction  $\hat{b}$ , Figure 3 left. The boom is installed on a tripod which has a 2 meter height above the ground on which the tripod rests. The lidar is installed below the reflected antenna, while the cameras are sited underneath the lidar. The lidar and cameras are oriented at elevation angle with respect to the horizontal  $\hat{b}$  [21]. The center camera's elevation angle  $\psi_1 = -45$  deg, while cameras 2 and 3 have elevation angles  $\psi_2 = \psi_3 = -36$  deg.

To compute the surface reflectivity, reflection point positions need to be computed relative to the reflected antenna, in order to compute the reflected antenna gain for each SPs  $(G_r)$ . Details about the reference frames, coordinate system construction and Fresnel zone transformations are found in [11] [12].

#### 2. Data Collection

In this work we present results from the last data campaign (Lake Michigan Test 11, see [11] [12]), which occurred on 21 February 2020. Figure 3 (right) shows a photo of the sensor system on-site and lake surface conditions. Figure 3 right displays a picture of the tripod while the tripod is mounted at the edge of the water with the boom extending out over the water. As seen from the photo, the surface is entirely water on the left side of the image, with a layer of ice to the center and right. There are visible breaks in the ice and thinner parts of ice where blue water is visible between sections of white ice. Figure 3 (left) shows a Google Map satellite image of the data collection site in Chicago on the shore of Lake Michigan, and the yellow arrows indicate the boom heading  $\hat{b}$ .

The system configuration and orientation details for data campaign (LM Test 11) are summarized in Table 1. This information

Data collection configuration	
Time	21 February 2020 11:58 CST
Sensor Position	latitude: 41.83798° N
	longitude:87.60612° W
Sampling rate $f_s$	5 MHz
RHCP antenna inline gain	30 dB
LHCP antenna inline gain	40 dB
USRP-direct RF gain	31 dB
USRP-reflected RF gain	31 dB
Boom heading $\mu$	$70^{\circ}$
Elevation angle of the reflected antenna $\kappa$	$-45^{\circ}$
Elevation angle of the lidar and central camera $\psi_1$	$-45^{\circ}$
Elevation angle of the cameras 2 and 3 $\psi_2$ and $\psi_3$	$-36^{\circ}$
Surface condition	Mixed ice and water

Table 1: Configurations of the Lake Michigan data collection campaign (LM Test 11).

was documented during the data campaign because, during post-processing, camera and lidar orientation angles are required for the transformation to create the map.



**Figure 3:** Left: Google Map satellite image of sensor location for data campaign (Lake Michigan Test 11). The yellow arrow defines the boom direction  $\hat{b}$ . Right: Photo of the experiment hardware setup, actual picture of the tripod, which is setup on the Lake Michigan 11.

# 3. Post-Processing

When the data campaign is completed at Lake Michigan, the collected GNSS, GNSS-R, lidar, weather station and camera data are brought to the lab for post-processing. Figure 4 describes the post-processing of data. In this Figure, green color indicates the "Verification" process, by which the true surface condition and type is established. The red steps are for GNSS-R detection. The verification process means that the complementary sensors' data are used to select PRNs whose reflection come from desired surface. To this end, sensor location and GPS almanac information are used to estimate satellites' position in ENU coordinate system. Next, the visible satellites' first Fresnel zone (i.e., specular point (SP)) is computed using Eq.(3) and lidar range information. Then, the ENU SP-lidar-camera Map is generated. To create the map, a camera's pixels in the camera image coordinate system are transformed to the ENU coordinate system, relative to the reflected antenna. For more details about the camera processing see [21]. Since GNSS-R captures from the reflected antenna, the ENU SP-lidar-camera map is transformed to the reflected antenna origin [12]. When the map's origin is the reflected antenna, satellites whose reflection comes from the

desired surface (ice and water) are manually selected. For selected satellites, the signal-to-noise ratio (SNR) is computed to calculate surface reflectivity via Eq.(1). In addition, the reflected antenna gain is needed for each pattern for SR computation, to find the antenna gain pattern see [11] [12]. The camera pixel's mean red value within the Fresnel zone of the satellite is used to detect ice. Because white ice corresponds to an RGB triplet of close to (1,1,1) and water will tend to have strong blue and green components, but not red, the red value of RGB is used as the metric for the presence of ice in the camera image.

Figure 5 shows the post-processing flow used to generate the ENU SP-lidar-camera map and compute the camera mean red value. As shown in this figure, two cameras' pixel positions are transformed into the east-north-up (ENU) system (the lidar is used as indicated in Figure 4 to provide depth information). The Fresnel zone and Specular Point (SP) of the selected satellites are computed using Eq. (3). Note that these equations represent the Fresnel zone in the plane of propagation. Then the FZ is transformed to the reflected antenna coordinate system ([15]) by rotating the plane of propagation using the azimuth angle of the satellite. Next, the FZs are mapped onto the ENU SP-lidar-camera map with origin at the reflected antenna. For a given satellite, the pixels that are inside the FZ are selected. The mean red value of the pixels inside the FZ are calculated. When the mean red value is found, it is compared with SR for each PRN to test the effectiveness of GPS SR at detecting ice.

To compute the SR using Eq. (1), the SNR is estimated based on Eq. (2). To calculate the maximum correlation power, data is coherently integrated for 1 ms then summed incoherently for 1 minute [22] [12]. When the SNR is found, the FZ center is computed using a satellite's location relative to the reflected antenna in ENU coordinates, and the lidar ranging information for the surface [12]. When the SPs and satellite's position are found relative to the reflected antenna,  $R_{ts}$  and  $R_{rs}$  are calculated. To compute the antenna gain  $G^r$ , the angle between a SP viewing direction and the body-zenith of the reflected antenna is computed. When the angle is found, the gain is computed from the reflected antenna gain pattern [11]. For details about the reflected antenna gain pattern calculation see [12] [11]. Now we have all parameters to estimate surface reflectivity.

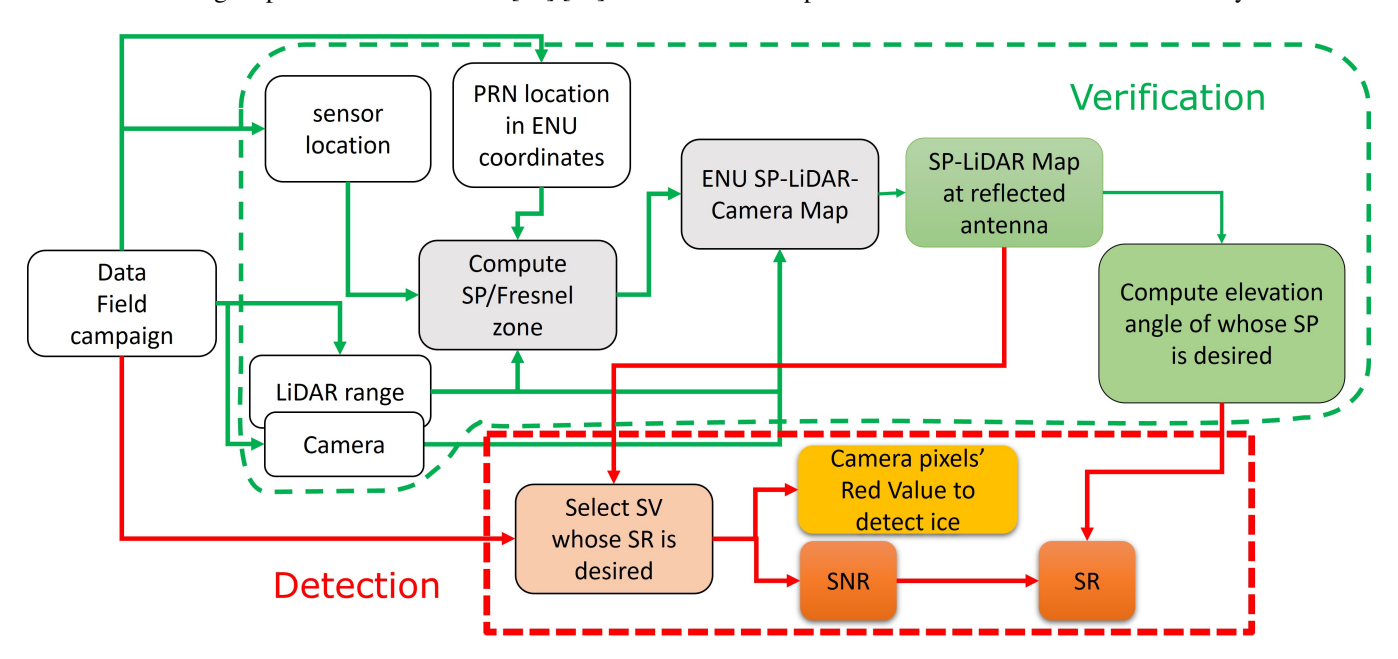


Figure 4: Post-processing flowchart, describing the process by which the surface type at a satellite PRN's specular point (SP) and Fresnel zone (FZ) are determined. Then the satellite (SV) is selected and its SNR and SR associated with the SP/FZ are computed

# IV. RESULTS

The surface of Lake Michigan was a heterogeneous mix of ice and water during data campaign (LM Test 11), as visible in Fig. 3 at right. The satellites in the sky at the start time of LM Test 11 are presented in the sky plot of Figure 6. Blue circles indicate satellites in the sky. Around the perimeter, zero indicates north of the sensor and 90 points east. At the center of circle is the zenith of the direct antenna. To estimate the satellites' ENU positions, a Yuma almanac [23] and approximate sensor position are used [11]. Since the boom is oriented to the east (Fig. 3 left), reflected signals of the satellites in the eastern part of the sky are anticipated to be on the lake surface. In particular, PRN 16 is at high elevation in the sky, and PRN 26's elevation is higher than the reflected antenna angle, such that the direct signal would be below the body-frame horizon of the antenna. In addition, the SP-lidar-camera map in ENU coordinates relative to the reflected antenna shows that the satellites in the eastern part of the sky are on the lake surface. The SP-lidar-camera map is used to visually select satellites for GNSS-R analysis.

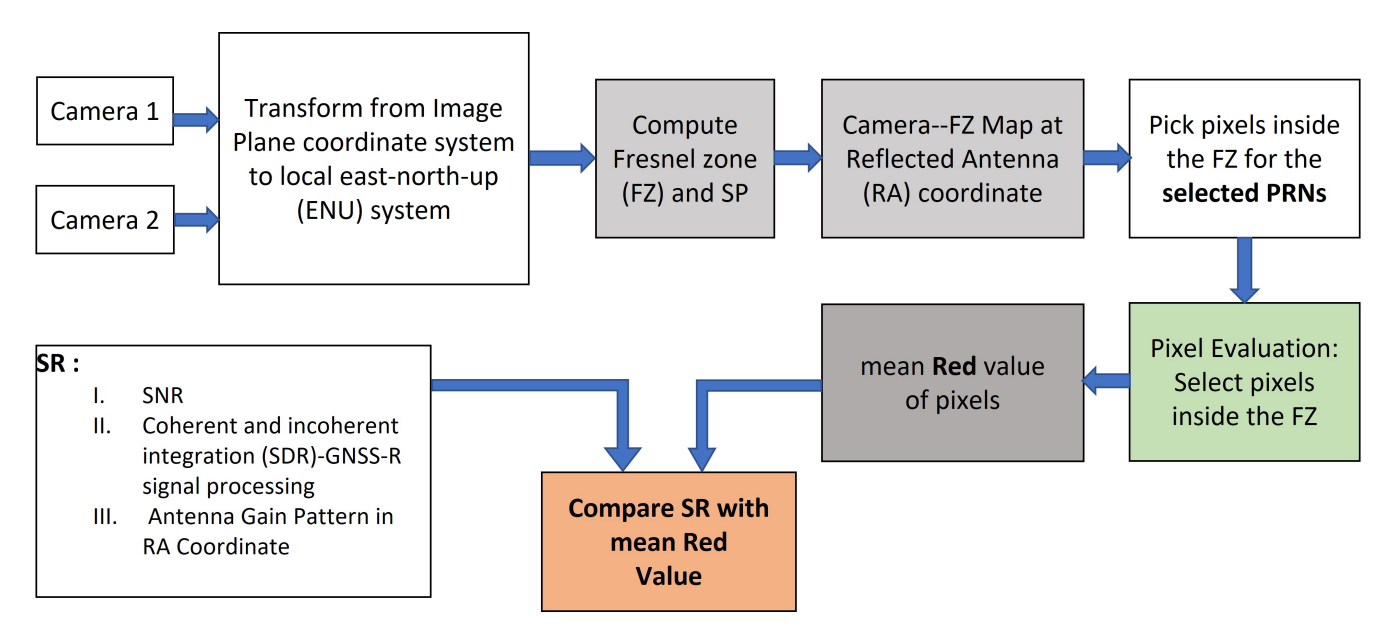


Figure 5: Post-Processing: Camera and SR

# #of visible SV on LM for Almanac Week 46 2-21-2020 at 11:57-11:58 CT 90 016

Figure 6: Yuma almanac-based sky plot at 11:58 Central Time (CT) for data campaign (LM Test 11)

Figure 7(a) shows the the SP-lidar-camera map in east-north coordinates relative to the reflected antenna. The green cross indicates the center of the reflected antenna, which is the origin of the map. The right (camera 3) and left (camera 2) cameras' pixels are mapped onto the ENU coordinates. The Fresnel zone ellipses of the PRNs whose SPs are on the surface are computed and mapped onto the camera pixels. The orange dots mark the SPs. The Fresnel zones of PRNs 16, 26, 27 and 31 are shown in Figure 7(a), each with a unique color.

Pixels selected for being inside the Fresnel zone are highlighted in Figure 7(b). PRN 16 and 26 are selected for further processing in this work, since their Fresnel zone scan through the desired surface during the 20 minute of data. Also, the majority of the

Fresnel zones of PRNs 16 and 26 are sampled by the cameras, such that their RGB values may be used for determining the surface type.

The surface reflectivity and mean red value (MRV) for PRN 16 are displayed in Figure 8. The left figure 8(a) is the SR value for PRN 16. In this figure, the horizontal axis is time in minutes since 11:58 local time, and the vertical axis is the SR value which is unitless. As seen in this figure, the SR for PRN 16 is fluctuating with time. The mean red value of pixels inside the Fresnel zone for PRN 16 is shown in Figure 8(b). The mean red value for PRN 16 is increasing with time. The correlation coefficient between SR and MRV for PRN 16 is  $\rho = 0.5341$ , which shows moderate correlation between SR and MRV for PRN 16. The moderate correlation may be due to a lack of overlap between the Fresnel zone of PRN 16 and the cameras' fields of view. In Figure 7 only slightly more than half of the ellipse has RGB pixels present, and these pixels skew toward the ice-containing part of the surface, even though the specular point itself is on the water (see Fig. 7(a)).

Figure 9(a) is the surface reflectivity (left) and the mean red value (right) for PRN 26 over time. As with Figure 9(a), the horizontal axis is minutes elapsed since 11:58 local time, and the vertical axis is the surface reflectivity (unitless). The SR for PRN 26 is increasing with time in this case. The mean red value for pixels inside the FZ for PRN 26 is plotted in Figure 9(b). The MRV value of PRN 26 also rises over time. The same trend is seen in both the SR and MRV. For PRN 26 the correlation coefficient is  $\rho = 0.9093$ , i.e., the SR of PRN 26 and MRV are highly correlated. It is notable that, at minute 13, both the SR and MRV drop then rise subsequently.

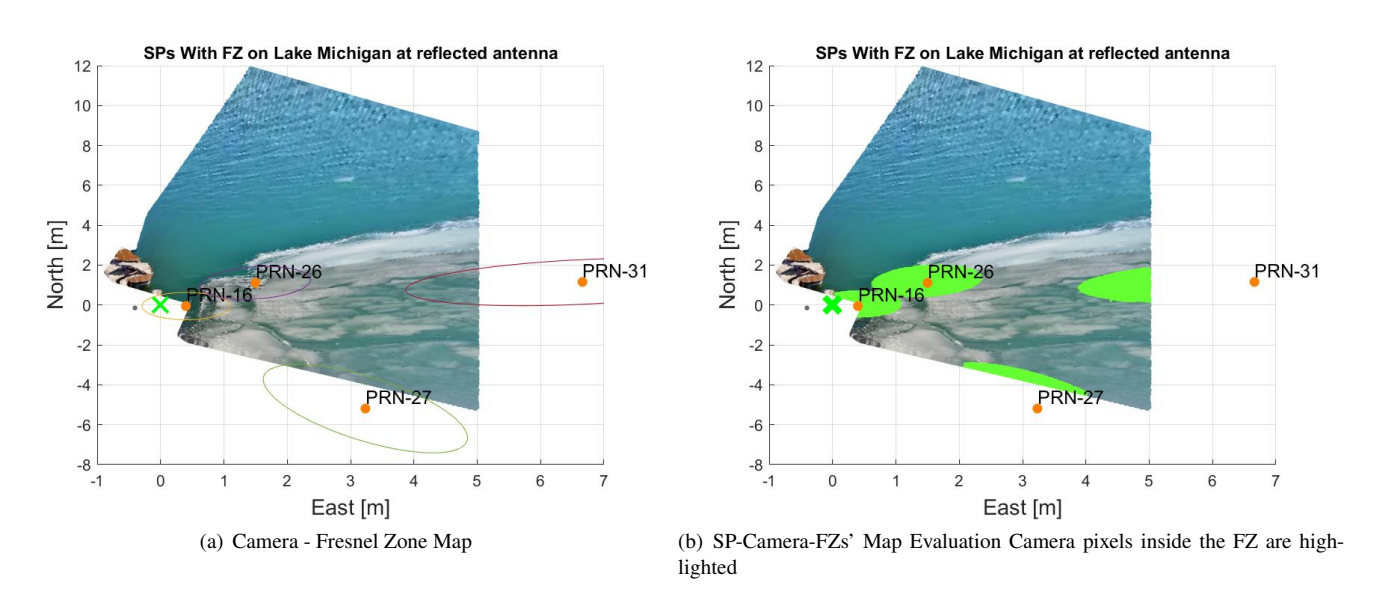


Figure 7: Fresnel zone mapping and camera pixel selection.

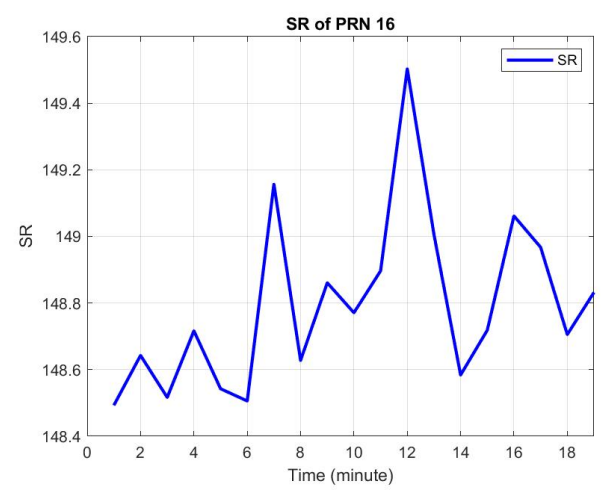
# V. CONCLUSION

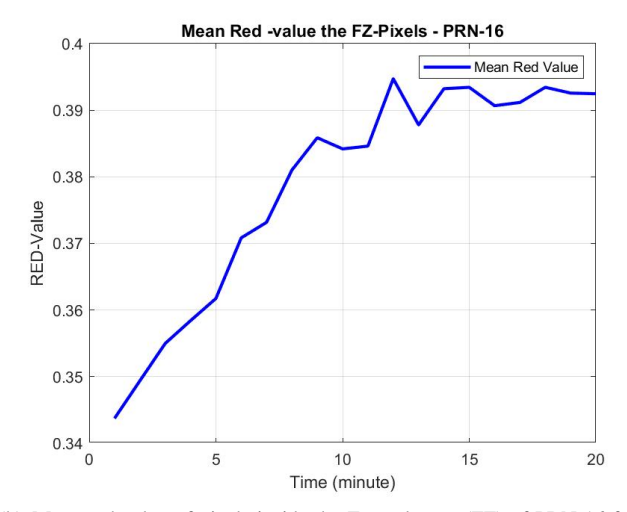
In this work, we correlated the GNSS-derived surface reflectivity with camera images to test whether GNSS-R surface reflectivity can distinguish ice from water. Results from a Lake Michigan data campaign that was held in Chicago, Illinois, in February 2020 at approximately  $(41^{\circ}50'23''N, 87^{\circ}36'15''\ W)$  are presented in this work. During this fieldwork the lake surface was mixed ice and water.

To compute the SR, 1 ms coherent integration of the correlation power is incoherently summed for 1 minute, and the Fresnel zone for PRNs whose SPs scan across both ice and water are computed. Pixels inside the FZ of each those PRNs are evaluated and selected to estimate the mean red value.

The SR of PRN 26 is highly correlated with camera RGB red value in the Fresnel zone. For PRN 16, a moderate correlation between SR and MRV is observed, which is attributed to the lack of enough camera pixels in the FZ. Part of the Fresnel zone of PRN 16 is beyond of our cameras' field of view, so the cameras do not provide enough RGB sampling about the entire Fresnel zone for PRN 16. Based on this study, we conclude that surface reflectivity of GNSS reflected signals can likely be used to distinguish ice from water.

In order to establish more conclusively about the SR of GNSS-R, in the future we will study additional PRNs whose Fresnel zones scan over ice and water, and additional correlations will be computed. Additionally, the SR and mean red value (MRV)





- (a) Surface reflectivity (SR) for PRN 16 for 19 minutes.
- (b) Mean red value of pixels inside the Fresnel zone (FZ) of PRN 16 for 20 minutes.

Figure 8: Comparison between surface reflectivity (SR) and mean red value for PRN 16.

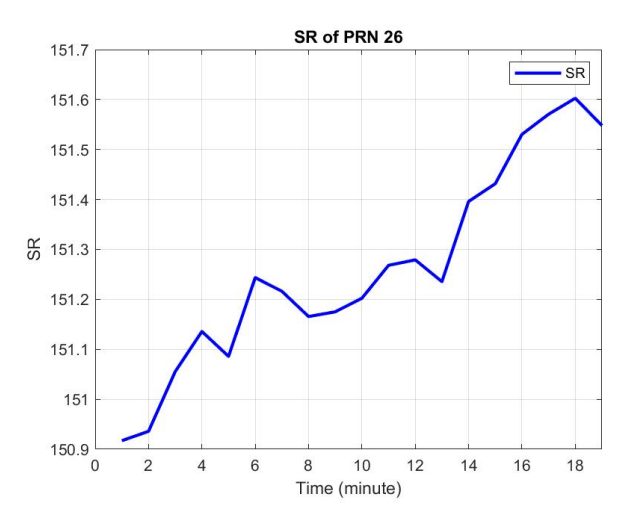
will be evaluated for each second rather than over a minute to test for increased sensitivity. The navigation message and GNSS direct signal will be used to improve the estimate of the Fresnel zone and sensor system location.

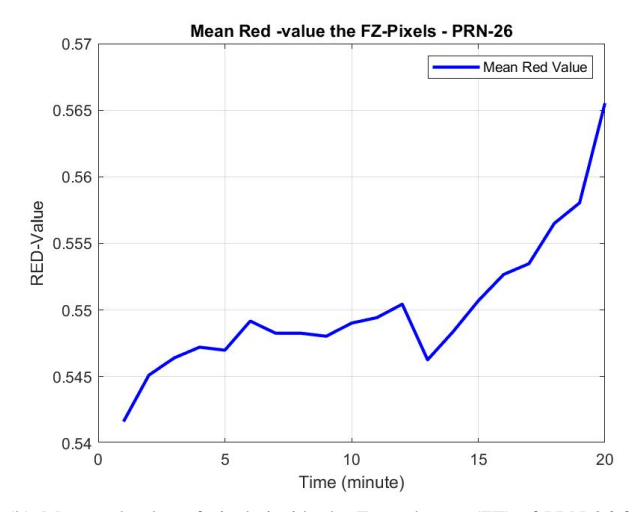
#### **ACKNOWLEDGEMENTS**

The authors thank David Stuart, Li Pan, and Aurora López Rubio for on-site help during the data campaigns. Thanks to the Chicago Park District for providing the Research Access Permit for all field tests. This work was funded by the National Aeronautics and Space Administration (NASA) award NNX15AV01G and National Science Foundation (NSF) award 1940483.

# REFERENCES

- [1] M. Martin-Neira, "A passive reflectometry and interferometry system (PARIS): Application to ocean altimetry," <u>ESA journal</u>, vol. 17, no. 4, pp. 331–355, 1993.
- [2] K. M. Larson and E. E. Small, "Estimation of snow depth using L1 GPS signal-to-noise ratio data," <u>IEEE Journal of Selected Topics in Applied Earth Observations and Remote Sensing</u>, vol. 9, no. 10, pp. 4802–4808, 2016.
- [3] M. Siegfried, B. Medley, K. Larson, H. Fricker, and S. Tulaczyk, "Snow accumulation variability on a west antarctic ice stream observed with GPS reflectometry, 2007–2017," Geophysical Research Letters, vol. 44, no. 15, pp. 7808–7816, 2017.
- [4] K. Edokossi, A. Calabia, S. Jin, and I. Molina, "GNSS-reflectometry and remote sensing of soil moisture: A review of measurement techniques, methods, and applications," Remote Sensing, vol. 12, no. 4, p. 614, 2020.
- [5] N. Rodriguez-Alvarez, X. Bosch-Lluis, A. Camps, M. Vall-Llossera, E. Valencia, J. F. Marchan-Hernandez, and I. Ramos-Perez, "Soil moisture retrieval using GNSS-R techniques: Experimental results over a bare soil field," <u>IEEE Transactions on Geoscience and Remote Sensing</u>, vol. 47, no. 11, pp. 3616–3624, 2009.
- [6] V. U. Zavorotny, S. Gleason, E. Cardellach, and A. Camps, "Tutorial on remote sensing using GNSS bistatic radar of opportunity," IEEE Geoscience and Remote Sensing Magazine, vol. 2, no. 4, pp. 8–45, 2014.
- [7] S. Gleason, "Remote sensing of ocean, ice and land surfaces using bistatically scanner GNSS signals from low earth orbit," Ph.D. dissertation, University of Surrey (United Kingdom), 2006.
- [8] N. G. Ruffini, F. Soulat, M. Caparrini, O. Germain, and M. Martín-Neira, "The eddy experiment: Accurate GNSS-R ocean altimetry from low altitude aircraft," Geophysical Research Letters, vol. 31, no. 12, 2004.
- [9] R. Pincus. The Climate Data Guide: Cloud observations from MODIS. R.Pincus And National Center for Atmospheric Research Staff (Eds). [Online]. Available: https://climatedataguide.ucar.edu/climate-data/cloud-observations-modis





- (a) Surface reflectivity (SR) for PRN 26 for 19 minutes.
- (b) Mean red value of pixels inside the Fresnel zone (FZ) of PRN 26 for 20 minutes.

Figure 9: Comparison between surface reflectivity (SR) and mean red value for PRN 26.

- [10] N. Snow and I. D. C. ". What are the limitations of MODIS data? | National Snow and Ice Data Center. National Snow and Ice Data Center. [Online]. Available: https://nsidc.org/support/21553418-What-are-the-limitations-of-MODIS-data-
- [11] R. Parvizi, "A novel remote sensing system using reflected GNSS signals," Ph.D. dissertation, Illinois Institute of Technology, 2020.
- [12] R. Parvizi, S. Khan, L. J. Pan, and S. Datta-Barua, "Surface reflectivity variations of GNSS signals from a mixed ice and water surface," in Proceedings of the 33rd International Technical Meeting of the Satellite Division of The Institute of Navigation (ION GNSS+ 2020), 2020, pp. 3909–3919.
- [13] R. Parvizi and S. Datta-Barua, "De-noising GNSS-reflectometry measurements from a freshwater surface," in <u>2019 URSI</u> Asia-Pacific Radio Science Conference (AP-RASC). IEEE, 2019, pp. 1–1.
- [14] W. Li, E. Cardellach, F. Fabra, S. Ribó, and A. Rius, "Measuring greenland ice sheet melt using spaceborne GNSS reflectometry from TechDemoSat-1," Geophysical Research Letters, vol. 47, no. 2, p. e2019GL086477, 2020.
- [15] H. D. Hristov, Fresnel Zones in Wireless Links, Zone Plate Lenses and Antennas. Artech House, Inc., 2000.
- [16] C. Chew, J. T. Reager, and E. Small, "CYGNSS data map flood inundation during the 2017 atlantic hurricane season," Nature Scientific Reports, vol. 8, no. 1, pp. 1–8, 2018.
- [17] P. Misra and P. Enge, "Special issue on global positioning system," <u>Proceedings of the IEEE</u>, vol. 87, no. 1, pp. 3–15, 1999.
- [18] K. M. Larson and F. G. Nievinski, "GPS snow sensing: results from the earthscope plate boundary observatory," GPS solutions, vol. 17, no. 1, pp. 41–52, 2013.
- [19] S. Datta-Barua, R. Parvizi, E. Donarski, S. Stevanovic, N. Wang, K. Herron, and B. Pervan, "Great lake surface characterization with GNSS reflectometry," in <u>Proceedings of the 29th International Technical Meeting of The Satellite Division of the Institute of Navigation (ION GNSS+ 2016)</u>, 2016, pp. 872–880.
- [20] R. Parvizi, H. S. Zadeh, L. Pan, B. Pervan, and S. Datta-Barua, "Multi-sensor study of lake michigan's surface using GNSS-reflectometry," in <u>Proceedings of the 31st International Technical Meeting of The Satellite Division of the Institute</u> of Navigation (ION GNSS+ 2018), 2018, pp. 2834–2847.
- [21] S. Khan, "3d reconstruction of lake surface using camera and lidar sensor fusion," Master's thesis, Illinois Institute of Technology, 2020.
- [22] R. Parvizi, J. Henry, N. Honda, E. Donarski, B. S. Pervan, and S. Datta-Barua, "Coordination of GNSS signals with lidar for reflectometry," in Proceedings of the 30th International Technical Meeting of The Satellite Division of the Institute of Navigation (ION GNSS+ 2017), 2017, pp. 3420–3433.

[23] U. C. G. N. Center. Navigation center. U.S. Department of Homeland Security. [Online]. Available: https://www.navcen.uscg.gov/?pageName=gpsAlmanacs